

Maximizing the potency of oxaliplatin coated nanoparticles with folic acid for modulating tumor progression in colorectal cancer

Ana Luiza C. de S.L. Oliveira ^{a,b,c}, Luana Zerillo ^{b,c}, Luis J. Cruz ^{b,*}, Timo Schomann ^{b,c}, Alan B. Chan ^c, Thaís Gomes de Carvalho ^{a,b,c}, Shirley Vitória de P. Souza ^d, Aurigena A. Araújo ^e, Lioe-Fee de Geus-Oei ^f, Raimundo F. de Araújo Júnior ^{a,b,c,d,g,*}

^a Postgraduate Program in Health Science, Federal University of Rio Grande do Norte (UFRN), Natal, RN, Brazil

^b Translational Nanobiomaterials and Imaging (TNI) Group, Radiology Department, Leiden University Medical Centrum, Leiden, the Netherlands

^c Percuros B. V, Leiden, the Netherlands

^d Graduation Student at Biomedical Sciences, Federal University of Rio Grande do Norte (UFRN), Natal, RN, Brazil

^e Postgraduate Program in Public Health and Pharmaceutical Science and Pharmacology, Department of Biophysics and Farmacology, Federal University of Rio Grande do Norte (UFRN), Natal, RN, Brazil

^f Department of Radiology, Leiden University Medical Center, Leiden, the Netherlands

^g Cancer and Inflammation Research Laboratory, Department of Morphology, Federal University of Rio Grande do Norte, 59064 741 Natal, RN, Brazil



ARTICLE INFO

Keywords:

Drug delivery system

Oxaliplatin

Folic acid

Apoptosis

Drug resistance

ABSTRACT

One of the challenges of nanotechnology is to improve the efficacy of treatments for diseases, in order to reduce morbidity and mortality rates. Following this line of study, we made a nanoparticle formulation with a small size, uniform surfaces, and a satisfactory encapsulation coefficient as a target for colorectal cancer cells. The results of binding and uptake prove that using the target system with folic acid works: Using this system, cytotoxicity and cell death are increased when compared to using free oxaliplatin. The data show that the system maximized the efficiency of oxaliplatin in modulating tumor progression, increasing apoptosis and decreasing resistance to the drug. Thus, for the first time, our findings suggest that PLGA-PEG-FA increases the antitumor effectiveness of oxaliplatin by functioning as a facilitator of drug delivery in colorectal cancer.

1. Introduction

Nowadays, cancer is one of the leading reasons for death worldwide. The number of incidence and mortality has increased in the last decades, and it is expected that the number will continue to grow [1,2]. Colorectal cancer (CRC), considered rare in the past, is now becoming more frequent and new therapeutical approaches are emerging to fight CRC, such as the use of nanomedicine to improve established therapies [3–5].

Tumor mass develops as a result of a sequence of malignant events, and some characteristics of the tumor cells are common to all types of tumor cells. One of them is the ability to prevent apoptosis [6,7]. Apoptosis is a biological process that occurs through the extrinsic and intrinsic pathways, converging on a common path that will end with cell death. The activation of these pathways helps to stop the progression of tumors [8,9].

Oxaliplatin (OXA) is a chemotherapeutic agent, a third-generation

platinum, that has been used in the treatment of CRC in therapeutic regimes [4,10,11]. This drug acts mainly against tumor cells by binding to DNA. Subsequently, OXA forms adducts in GC-rich areas in the DNA, activating the DNA replication and transcription processes [12,13]. Mechanisms of resistance to OXA are reported as one of the major causes of failure in the treatment of CRC, due to the accumulation of enzymes and detoxification transporters (leading to increased detoxification), resulting in decreased intracellular amount of drugs and accumulation of repair enzymes by excision of nucleotides [11,12,14].

Drug delivery systems (DDSs) may be used to overcome the limitations of OXA treatment. This can be realized by adjusting the dose of the chemotherapeutic agent, increasing the internalization of the drug in the cells and enhancing bioavailability, which will lead to increased drug efficiency, and a decrease in adverse effects and drug resistance [15–17]. Currently, poly (D,L-lactide-co-glycolic acid) (PLGA) is widely used as a DDS due to its biocompatibility and biodegradability characteristics

* Corresponding authors at: Translational Nanobiomaterials and Imaging, Department of Radiology, Bldg.1, C2-187h, Leiden University Medical Centre, Albinusdreef 2, 2333 ZA Leiden, the Netherlands.

E-mail addresses: l.j.cruz_ricondo@lumc.nl (L.J. Cruz), araujojr@cb.ufrn.br (R.F. de Araújo Júnior).

[18,19]. PLGA polymer nanoparticles can be designed with surface modifications; an example is the addition of hydrophilic and polymeric polyethylene glycol (PEG), which prevents interactions with macrophages or phagocytes, guaranteeing the delivery and distribution of drugs in the tumor environment [18–21]. These nanoparticles can have their surfaces modified with the addition of targeting molecules, which increases the selectivity, applicability and effectiveness of DDS [22]. An example for a nanoparticle targeting is folic acid (FA), that interacts with the folate receptor, which is overexpressed in a wide range of human cancers, but is very low in healthy tissues [21,23]. Targeted PLGA nanoparticles have been used in the development of a DDS for the treatment of cancer; they improve the antitumor activity of drugs by

inducing apoptosis, reducing side effects, suppressing metastasis, and decreasing resistance to drugs [4,5].

Based on the above, the aim of this study is to formulate a novel modified FA-PLGA nanoparticles loaded with OXA to enhance the effect of this drug against colorectal cancer. Our nanoparticle system can target CRC cells and amplify the anti-tumor activity of OXA. In this study, for the first time we combined PLGA, FA, and OXA, we designed, characterized, and evaluated anti-tumor activity in murine colon carcinoma cells of the modified FA-PLGA nanoparticles loaded with OXA.

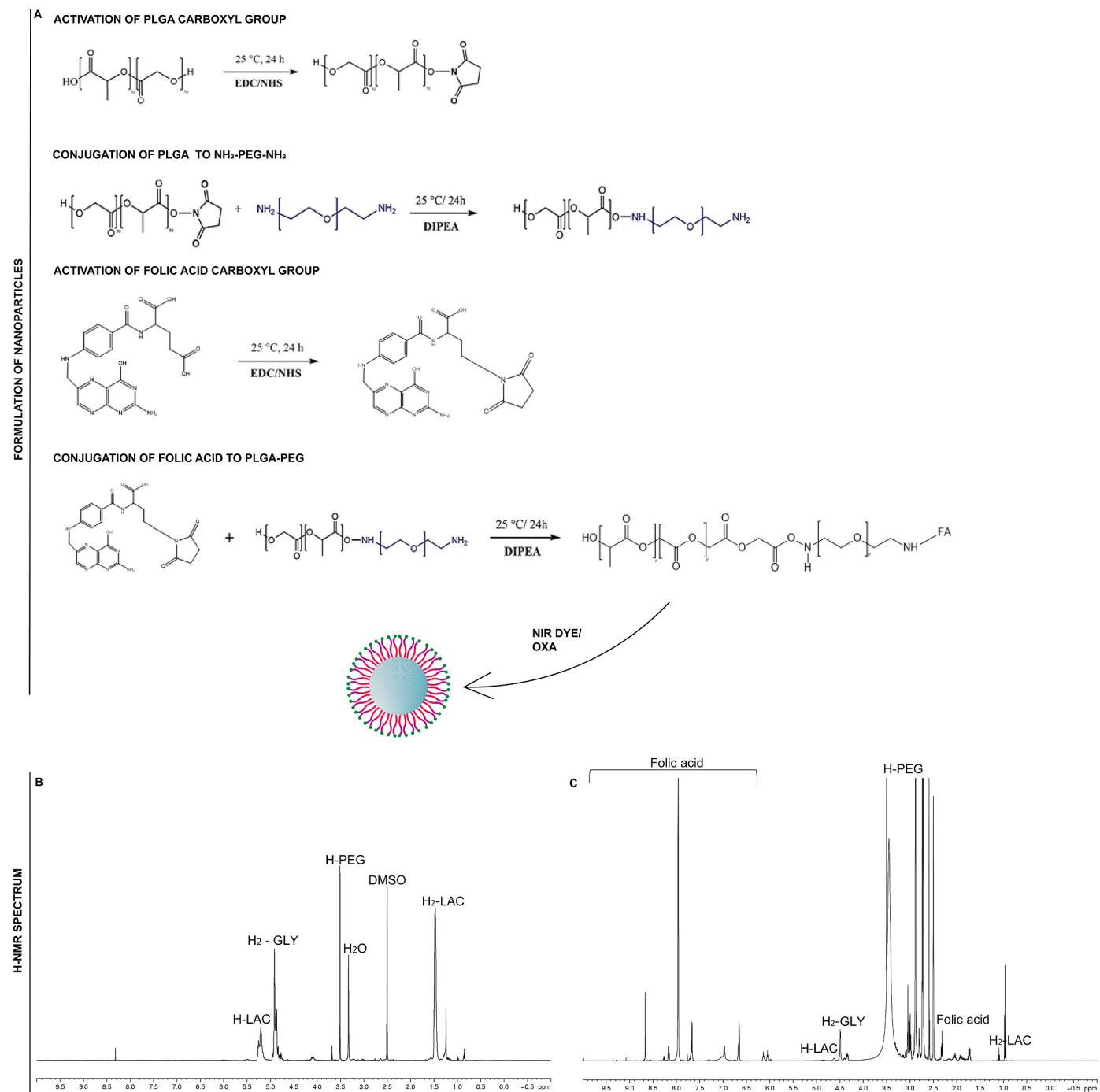


Fig. 1. Formulation and characterization of nanoparticles. (A) Schematic illustration of formulation of PLGA-PEG-FA co-polymer and nanoparticles. H-NMR spectrum: (B) PLGA-PEG and (C) PLGA-PEG-FA co-polymers.

2. Materials and methods

2.1. Reagents

PLGA (PURASORB® PDLG 5002A 50:50, inherent viscosity 0.20 dL/g, MW = 17,000) was obtained from Carbion PURAC (Amsterdam, the Netherlands); polyvinyl alcohol (PVA) (87–89% hydrolyzed, typical MW 13,000–23,000), N-(3-dimethylaminopropyl)-N'-ethylcarbodiimide hydrochloride (EDC, ≥98.0%), N-hydroxysuccinimide (NHS, 98%), methylene chloride, dimethylformamide (≥99.8%), chloroform (≥99%), and triethylamine (TEA, ≥99.5%) were purchased from Sigma-Aldrich (Steinheim, Germany). PEG with diamine group (NH₂-PEG-NH₂, MW = 3143) was obtained from Iris Biotech (Biotech GmbH, Marktredwitz, Germany). The solvent used to prepare the nanoparticles, and dichloromethane (DCM, ≥99.8%) were purchased from Sigma-Aldrich (Darmstadt, Germany). The NPs were all loaded with NIR dye (IR-780 Iodide) purchased from Sigma-Aldrich (Zwijndrecht, the Netherlands) and OXA (Sigma-Aldrich, Darmstadt, Germany). The target FA was obtained from Sigma-Aldrich (Steinheim, Germany). The *in vitro* studies were performed using Dulbecco's modified Eagle's medium (DMEM) (Gibco Laboratories, Grand Island, USA), Fetal Bovine Serum (FBS) (Bodinco BV, Alkmaar, the Netherlands), trypsin/EDTA (Gibco Technologies, Grand Island, NY, USA), CellTiter 96 AQueous One Solution (MTS) solution (Promega Corporation, Madison, WI, USA), 4,6-diamidino-2-phenylindole (DAPI) (Thermo Fisher Scientific, Cambridge, MA, USA), DiD cell-labeling solution (Thermo Fisher Scientific, Cambridge, MA, USA), V-FITC (BD Pharmigen, CA, USA), To-pro 3 iodide (642/661) (Invitrogen, Eugene, USA) and Tween-20 (Promega, Madison, WI, USA). All primary and the secondary antibodies were purchased from Abcam, Burlingame, CA, USA. The *in vivo* studies were performed using streptavidin/Haptoglobin Related Protein (HRP)-conjugated secondary antibody (Biocare Medical, Concord, CA, USA), colorimetric-based detection kit (TrekAvidin-HRP Label + Kit from Biocare Medical, Pacheco, USA), trizol reagent (Invitrogen Co., Carlsbad, CA, USA), SV Total RNA Isolation System (Promega, Madison, WI, USA) and SYBR Green Mix in the Applied Biosystems 7500 FAST system (Applied Biosystems, Foster City, CA, USA).

2.2. Synthesis of polymers as well as preparation and characterization of nanoparticles

The polymers PLGA-PEG and PLGA-PEG-FA were synthesized in 4 different steps (Fig. 1A) using the single-emulsion solvent evaporation method [24], and were characterized by H-NMR (Proton nuclear magnetic resonance). For the nanoparticles loaded with near infrared 780 dye (NIR) and co-loaded with OXA, a double-emulsion solvent evaporation method of water-oil-water (W/O/W) was used [25].

An optical measure was performed to test the amount of FA conjugated with PLGA-PEG as follows: a solution of PLGA-PEG-FA was measured with Amersham Biosciences Ultrospec 2100 pro, UV/Vis Spectrophotometer and Absorbance was read at 350 nm [26,27].

In order to determine the encapsulation efficiency [28] and the loading content of the NIR dye and OXA, a solution of nanoparticles was measured for the NIR dye content using an Odyssey Infrared Imager 9120 (LI-COR) scanner at 800 nm. The concentration of OXA was determined by reversed-phase high-performance liquid chromatography (RP-HPLC).

2.3. Morphology and physicochemical properties of nanoparticles

To visualize and characterize the structure of the nanoparticles, transmission electron microscopy (TEM) was used. A droplet of 3 µL of the nanoparticle solution was imaged in a Tecnai 12 Biotwin transmission electron microscope (FEI, the Netherlands), equipped with a LaB6 filament operated at 120 kV. The average size of the nanoparticles and their polydispersity index (PDI) were determined by dispersing the

nanoparticles in MilliQ water using Dynamic Light Scattering (DLS). The stability of the nanoparticles was determined by measurement of their zeta potential (Zetasizer Nano S90, Malvern Instruments, Worcestershire, UK). The zeta potential analysis of the nanoparticles was performed by DLS.

2.4. Drug release studies

The *in vitro* drug release of OXA from PLGA nanoparticles was evaluated in phosphate-buffered saline (PBS) with pH = 7.4 as release medium. Briefly, 1 mg of the freeze-dried nanoparticles [PLGA-PEG OXA and PLGA-PEG (OXA)-FA] were resuspended in PBS (1 mg/mL), triplicate for each formulation, and incubated at 37 °C under continuous shaking (300 rpm). At predetermined time points the nanoparticles were separated by centrifugation (12,000 rpm for 20 min), 150 µL aliquots were sampled and 150 µL of fresh and warm PBS added to release medium. The aliquots were maintained at –20 °C and, at the end of experiment, the concentration of OXA in the supernatant was measured spectrophotometrically at λ = 240 nm (Ultrospec 2100 pro).

2.5. Binding assay and uptake assay

Murine colorectal carcinoma (CT-26) cells were seeded in a black-walled 96-well cell culture microplate and incubated with PLGA-PEG and PLGA-PEG-FA at 10 µg/mL for 0, 1, 2, 8, or 24 h. For the binding assay, the plate was maintained at 4 °C, while the plate was maintained at 37 °C for the uptake assay. After the different time points, nuclei of the cells were stained with To-pro 3 iodide dye, which is detectable at 700 nm. The plate was imaged with an Odyssey Infrared Imager 9120 (LI-COR) scanner using 700 nm and 800 nm channels to visualize the cell nuclei and NIR-loaded nanoparticles, respectively.

2.6. Internalization of nanoparticles by cells and fluorescence imaging

The CT-26 cells were plated and treated with PLGA-PEG and PLGA-PEG-FA at 10 µg/mL. After 4, 8, 24, and 48 h, the cells were stained with DiD and DAPI. For the visualization of nanoparticles (yellow), cell membrane (pink), and nucleus (blue), a Leica DM5500 B fluorescence microscope equipped with a Leica DFC365 FX digital camera (Leica) was used. Digital images were acquired, analyzed, and stored using Leica Application Suite X (LAS X) software.

2.7. Viability test

The cells were cultured and free OXA, PLGA-PEG, PLGA-PEG (OXA) and PLGA-PEG-FA (OXA) at concentrations of 1 µg/mL, 5 µg/mL, 10 µg/mL, 20 µg/mL, and 50 µg/mL, respectively, were added; positive (25% DMSO) and negative controls were included. After 24, 48 or 72 h of treatment, MTS [3-(4,5-dimethylthiazol-2-yl)-5-(3-carboxymethoxyphenyl)-2-(4-sulfophenyl)-2H-tetrazolium, inner salt] solution was added to the wells and incubated for 3 h. Absorbance was measured at 490 nm using Molecular Devices VERSAmax Tunable Microplate Reader.

2.8. Detection of cell death by flow cytometry and immunofluorescence

CT-26 cells were plated and treated with free OXA and PLGA nanoconjugates [PLGA-PEG (OXA) and PLGA-PEG-FA (OXA)] at 10 µg/mL and 20 µg/mL for 24 and 48 h. After each period, the cells intended for flow cytometric analysis were labelled with Annexin V-FITC and DAPI, sorted with a BD FACS Canto II (BD Biosciences, CA, USA), and analyzed with FlowJo software, version 10.1 (Tree Star Inc., CA, USA). For immunofluorescence, the cells were incubated with the primary antibodies, anti-FAS-associated protein with death domain (FADD) rabbit (2.5:100), anti-apoptotic protease activating factor 1 (APAF-1) rabbit (1:100), and anti-caspase-3 rabbit (1:200), in blocking solution at 4 °C

overnight. The primary antibody was detected with Alexa Fluor 555 anti-rabbit secondary antibody diluted at 1:300 in blocking buffer. DAPI (1:1000) in phosphate-buffered saline was used for nuclear staining. Samples were examined with a Leica DM5500 B fluorescence microscope, as mentioned above.

2.9. CRC xenograft *in vivo* models and treatment regimens

For the animal model, the CT-26 cells (5×10^6) was subcutaneously injected into the right flank of male Balb/c mice. When the tumor volume achieved 3–4 mm [29], the animals were organized into four groups with five animals each, and were treated intratumorally three times in 15 days with injection dose of 5 mg/Kg. The groups for this experiment were, (1) Saline = 5 mg/Kg saline solution, (2) OXA = 5 mg/Kg, (3) PLGA-PEG (OXA) = 5 mg/Kg and (4) PLGA-PEG-FA (OXA) = 5 mg/Kg. The tumor size was measured every two days during 21 days or until the tumor reached a volume of 2000 mm³ [30,31]. For calculate their volume, was used the equation below [32]:

$$\text{Volume} = (\text{length} \times \text{width}^2 \times 0.523) \quad (1)$$

In the end of the experiment the animals were euthanized (80 mg/Kg, i.p.) 2% thiopental (Cristália, São Paulo, Brazil) and the subcutaneous tumor was removed and collected, half of the tumor was immediately stored at -80 °C for qPCR analysis and the other part were placed in 10% paraformaldehyde for histopathological analysis. Therefore, the protocol was accepted by the Committee on the Ethics of Animal Experiments of the UFRN (Universidade Federal do Rio Grande do Norte) (CEUA, permit number: 222.011/2020).

2.10. Immunohistochemical staining of caspase-3 and survivin

The tumors of each group were cut using a microtome. Tissue sections were stored with primary antibodies anti-caspase-3 (CUSABIO CSB-PA 140280) and anti-survivin (NOVUS NB 500-201SS) at 4 °C overnight. Then, the fragments were washed with phosphate-buffered saline and incubated with a streptavidin/haptoglobin-related protein (HRP)-conjugated secondary antibody.

The proteins showed immunoreactivity with the use of colorimetric-based detection kit following the protocol provided by the manufacturer. To obtain digital images, a high-power objective (40×) light microscopy (Nikon Eclipse 2000 equipped with Nikon DS-Fi2; Nikon Corporation, Tokyo, Japan) was used. For analysis the intensity of cell immunostaining, two trained examiners in a double-blind evaluated the labelling intensity. The immunoreactivity was analyzed based on the scores with minor modifications [33] for which the and the percentage (P) of tumor cells with characteristic staining (from an undetectable level or 0%, for homogeneous staining or 100%) and estimate of the intensity (I) of staining (1, weak staining; 2, moderate staining; and 3, strong staining). The result of the scores is obtained by multiplying the value of the percentage of cells marked by the intensity of the mark.

2.11. Analysis of mRNA expression

The RNA extraction from tumor tissue was realized using a trizol reagent and SV Total RNA Isolation System. For real-time quantitative polymerase chain reaction (PCR) analyses, a SYBR Green Mix was used in the β-actin, FADD, APAF-1, multidrug resistance protein 1 (MDR1), survivin, C-X-C chemokine receptor type 4 (CXCR4), and monocyte-derived chemokine (CCL22) messenger ribonucleic acids (mRNAs). The primers are listed in Table S1.

The standard PCR conditions were followed [4]. Mean threshold cycle (C_t) values were used to calculate the relative expression levels of the target genes for the experimental groups, relative to those in the negative control group; expression data were normalized relative to the housekeeping gene β-actin using the $2^{-\Delta\Delta C_t}$ formula.

2.12. Statistical analysis

All *in vitro* experiments were performed in triplicate. The significant differences between the groups were calculated using the analysis of variance (ANOVA) and the Bonferroni's test, as indicated. A *p*-value of <0.05 was considered to be statistically significant (*p* < 0.05, *p* < 0.01, *p* < 0.001, and *p* < 0.0001).

3. Results

3.1. Synthesis and characterizations of nanoparticles

The success of PLGA-PEG and PLGA-PEG-FA polymers was confirmed by H-NMR analysis. It was possible to identify the PLGA groups [-CH₂- and -CH₃ peaks of poly(D,L-lactide), *d* = 5.2–5.3 and 1.5 ppm; -CH₂- peak of poly(glycolide), *d* = 4.8–4.9 ppm], the PEG group (*d* = 3.6 ppm), and the characteristic peaks of the folic acid (*d* = 4.5, 6.6, 7.6, and 8.6 ppm) (Fig. 1B and C).

The average size, the zeta potential and the percentage encapsulation efficiency of the nanoparticles are displayed in Table 1, and the DLS curves at Supplementary materials (Fig. 1S). All nanoparticles were negatively charged as determined by measurement of their zeta potential. In average, 64.68% percent of FA was conjugated to PEG-PLGA as well as 64.06% conjugated to PLGA-PEG-FA (OXA). The percentage of encapsulation efficiency of OXA for PLGA-PEG NPs was 55% and for PLGA-PEG-FA nanoparticles it was 50% (Table 1).

The morphology of the nanoparticles was visualized by TEM microscopy and revealed that all generated nanoparticles were spherical, with a smooth surface and uniform sizes (Fig. 2A–D).

3.2. Drug release studies

The PLGA-PEG system demonstrating through the results obtained slow, gradual and progressive release. The release study of OXA from PLGA-PEG (OXA) and PLGA-PEG-FA (OXA) in PBS initially showed different patterns with about 16% of OXA released within the first 24 h for PLGA-PEG-FA (OXA) and 7% of OXA for the PLGA-PEG (OXA) (Fig. 2F). However, after 8 days, PLGA-PEG-FA (OXA) started released slowly then PLGA-PEG (OXA). The OXA release for was 100% around 23 days, while until the end of the experiment (28 days), the PLGA-PEG-FA (OXA) did not release all amount of OXA (Fig. 2E).

3.3. Binding and uptake assay

In Fig. 3, the nanoparticle with the target FA (PLGA-PEG-FA) showed higher binding and uptake than the nanoparticle without the target FA (PLGA-PEG). For binding assay there is no statistical difference between

Table 1

Diameter, polydispersity index, zeta potential, percentage of FA bound to PLGA-PEG as well as encapsulation efficiency (EE%) of NIR dye and OXA in the analysis of the chosen nanoparticles.

NPs	Size ± SD (nm)	PDI	Zeta potential ± SD (mV)	% FA bound to PLGA-PEG	EE% NIR	EE% OXA
PLGA-PEG	197.3 ± 0.52	0.01	-20.1 ± 5.09	-	39.03	-
PLGA-PEG (OXA)	198.5 ± 0.67	0.04	-20.8 ± 4.07	-	37.14	55
PLGA-PEG-FA	180.8 ± 1.35	0.04	-24.5 ± 5.07	64.68	26.05	-
PLGA-PEG-FA (OXA)	201.3 ± 1.78	0.06	-23.6 ± 9.51	64.06	24.09	50

Notes: PDI (Polydispersity Index), nm (Nanometer), Standard Deviation (SD), Millivolt (mV).

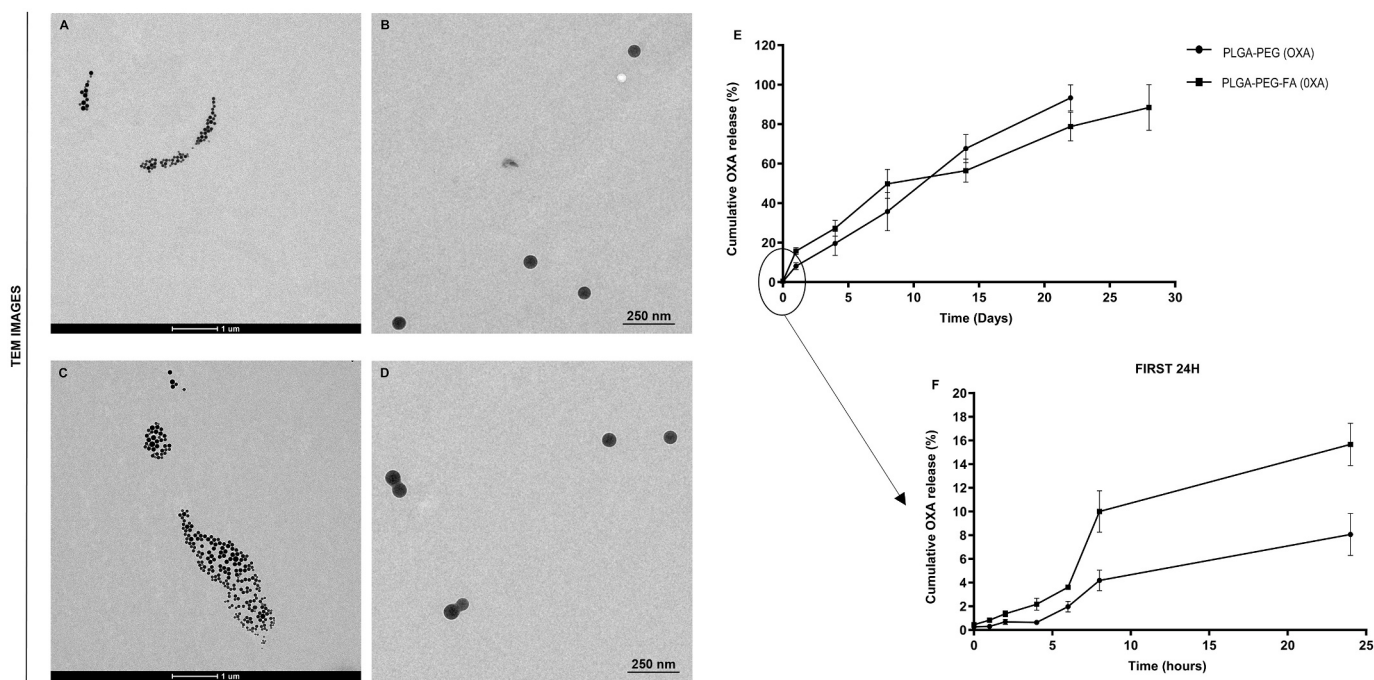


Fig. 2. Morphology images, and Drug release studies of nanoparticles. Morphology images of nanoparticles obtained by TEM: (A, B) PLGA-PEG (OXA) and (C, D) PLGA-PEG-FA (OXA). The graphs show the percentage of cumulative release of OXA in PBS, when the drug is encapsulated in two systems, PLGA-PEG and PLGA-PEG-FA. (E) Cumulative release throughout the experiment. (F) Cumulative release in the first 24 h of the experiment.

the nanoparticles at time 0 h, but all other times presented differences between them. For 1 h, $p < 0.001$; for 2 h $p < 0.01$; for 4 h, 8 h and 24 h the difference is $p < 0.0001$. While for the uptake there is no difference between the nanoparticles at time 0 h and 24 h, for the others time points the difference has a $p < 0.0001$ for 1 h and 2 h, $p < 0.001$, for 4 h and $p < 0.01$ for 8 h (Fig. 3).

3.4. Internalization of nanoparticles

The images show both nanoparticle formulations inside the tumor cells (in yellow) at all time points. However, Fig. 3 shows that more PLGA-PEG-FA nanoparticles than the PLGA-PEG were able to enter the tumor cells (Fig. 3).

3.5. Viability test

PLGA-PEG did not show cytotoxicity at any time point (Fig. 2S). After 24 h, the free OXA showed cytotoxicity at 5, 10, 20 and 50 $\mu\text{g}/\text{mL}$ ($p < 0.0001$), PLGA-PEG (OXA) showed similar cytotoxicity than OXA ($p < 0.001$ at 5, 10 and 50 $\mu\text{g}/\text{mL}$ and $p < 0.001$ for 20 $\mu\text{g}/\text{mL}$). The activity of PLGA-PEG-FA (OXA) was detected at all concentration ($p < 0.0001$), also at the lower dose, 1 $\mu\text{g}/\text{mL}$ (Fig. 2SA). After 48 h, treatment with free OXA, PLGA-PEG (OXA) and PLGA-PEG-FA (OXA) at all concentrations further decreased the number of viable cells [$p < 0.0001$, except for 1 $\mu\text{g}/\text{mL}$ OXA ($p < 0.01$)] (Fig. 2SB). After 72 h of treatment, the result was comparable, but 1 $\mu\text{g}/\text{mL}$ OXA did not show significant cytotoxicity (Fig. 2SC).

3.6. Flow cytometry

The data showed that only PLGA-PEG-FA (OXA) induced cell death at a concentration of 20 $\mu\text{g}/\text{mL}$ ($p < 0.001$) after 24 h compared to the control (Fig. 4A). After 48 h, the percentage of cell death for the three compounds was higher than that of the control. The activity of 10 $\mu\text{g}/\text{mL}$ OXA and 10 $\mu\text{g}/\text{mL}$ PLGA-PEG (OXA) was higher ($p < 0.0001$) than 20 $\mu\text{g}/\text{mL}$ OXA, 20 $\mu\text{g}/\text{mL}$ PLGA-PEG (OXA) and 10 $\mu\text{g}/\text{mL}$ and 20 $\mu\text{g}/\text{mL}$

PLGA-PEG (OXA) ($p < 0.01$) (Fig. 4B). Treatment groups [OXA, PLGA-PEG-FA (OXA) and PLGA-PEG (OXA)-FA] were compared at the same concentration (10 $\mu\text{g}/\text{mL}$) and same treatment time (48 h), the result were that PLGA-PEG-FA (OXA) induced more cell death than others samples in the same condition, $p < 0.5$ for comparison with OXA and $p < 0.001$ for comparison with PLGA-PEG-FA (OXA) (Fig. 4B).

3.7. Immunofluorescence

To analyze the apoptosis pathway induced by nanoparticles, cells were labelled with fluorescent antibodies and subsequently imaged. After 24 h of treatment, only 10 $\mu\text{g}/\text{mL}$ and 20 $\mu\text{g}/\text{mL}$ PLGA-PEG-FA (OXA) induced apoptosis through the extrinsic route (FADD) and intrinsic route (APAF-1) compared to the negative control. Regarding the common route (caspase-3), only OXA and PLGA-PEG (OXA) at a concentration of 10 $\mu\text{g}/\text{mL}$ did not show a significant difference when compared with the control. However, 20 $\mu\text{g}/\text{mL}$ PLGA-PEG-FA (OXA) showed a significant difference between treatments when compared to OXA and PLGA-PEG (OXA) at the same dose ($p < 0.001$) (Figs. 4C–E and 5).

After 48 h, all three formulations of both doses induced statistically significant apoptosis via the extrinsic route (FADD) and intrinsic route (APAF-1) when compared to the control group, with the exception of PLGA-PEG (OXA) at 20 $\mu\text{g}/\text{mL}$. The intensity of the fluorescence intensity of FADD labelling of cells treated with 20 $\mu\text{g}/\text{mL}$ PLGA-PEG-FA (OXA) was increased when compared to the other two treatments, OXA and PLGA-PEG (OXA), at the same concentration ($p < 0.0001$). Caspase-3 detection results showed that only OXA in both concentrations ($p < 0.5$) and PLGA-PEG-FA (OXA) at 20 $\mu\text{g}/\text{mL}$ ($p < 0.001$) induced apoptosis. It is worth noting that when comparing 20 $\mu\text{g}/\text{mL}$ of free OXA with PLGA-PEG-FA (OXA) there is a difference between these treatments, showing greater apoptosis induction by the nanoparticle DDS ($p < 0.5$; Fig. 4F–H and 5).

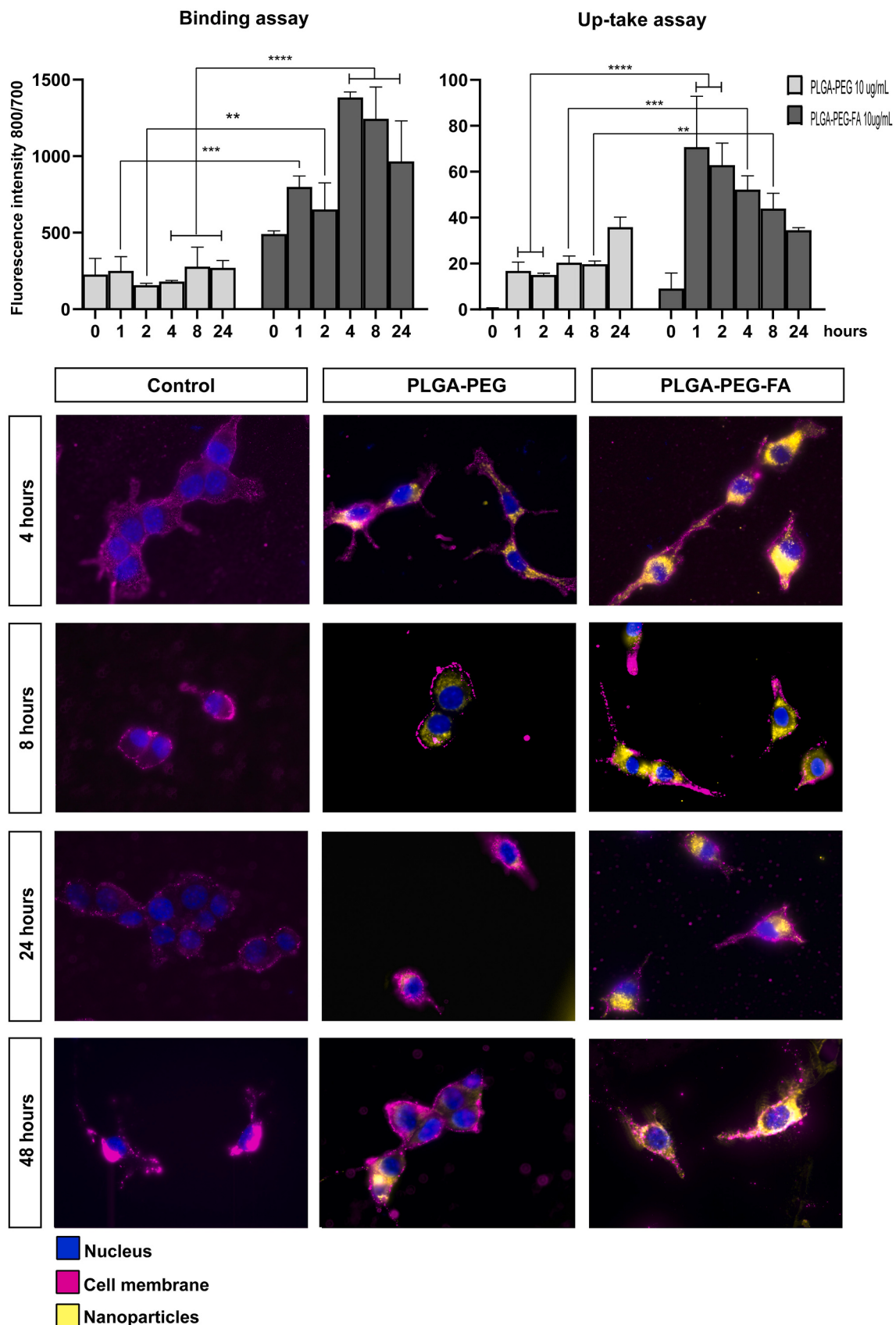


Fig. 3. Binding, uptake, and Internalization assays of nanoparticles by CT-26 cells. The graphs show the fluorescence intensity (y axis) for the dye contained in the nanoparticles when the cells are treated with 10 µg/mL PLGA-PEG and PLGA-PEG-FA for several hours (x axis). The images show the PLGA-PEG and PLGA-PEG-FA nanoparticles (in yellow) at a concentration 10 µg/mL inside the cancer cells after 4, 8, 24, and 48 h of incubation. Pink: membrane. Blue: nucleus. Magnification: 63×. (For interpretation of the references to colour in this figure legend, the reader is referred to the web version of this article.)

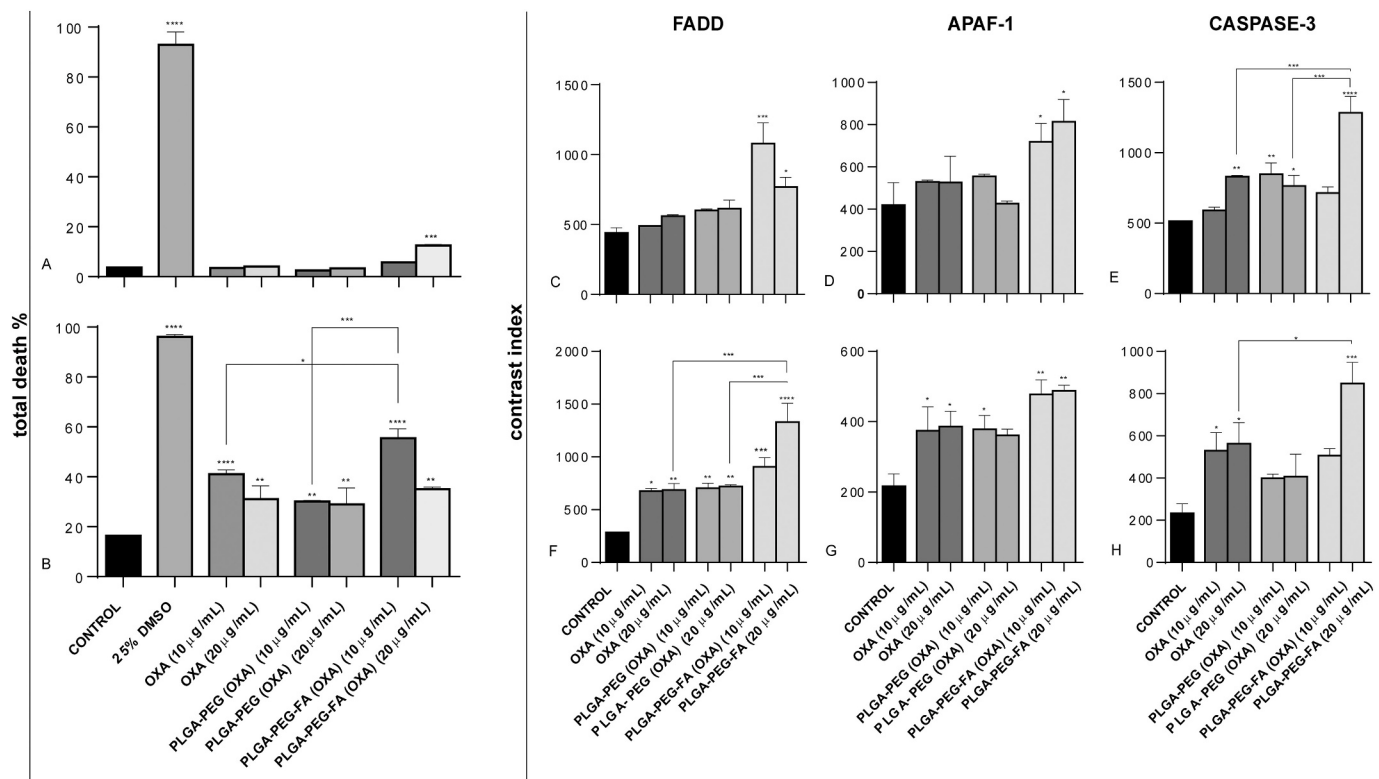


Fig. 4. Total death, and Contrast index for immunofluorescence. The graph A and B displays the total cell death after 24 h (A) and 48 h (B) of treatment. The contrast index for FADD, APAF-1, and caspase-3 of CT-26 after treatment with the nanoparticles and free OXA for 24 h (C, D and E, respectively) and for 48 h (F, G and H, respectively) are displayed. * $p < 0.05$, ** $p < 0.01$, *** $p < 0.001$, and **** $p < 0.0001$.

3.8. In vivo study

The *in vivo* model was applied to analyze the activity of the nanoparticulate systems and compare them with the free drug in relation to apoptosis, drug resistance, and metastasis factors. The macroscopic results showed a tumor growth curve with a difference in all treated groups in relation to the saline group (negative control), with $p < 0.0001$ (Fig. 6A-E). Tumor weight decreased considerably among the treated groups, which was contrary to the saline group ($p < 0.0001$). There was also a significant difference between the treatment with free OXA and PLGA-PEG-FA (OXA) ($p < 0.01$; Fig. 6F).

For analysis of the tumors, immunohistochemistry and RT-PCR were applied. Immunohistochemical analyses showed that all treated groups had low expression of survivin compared to the saline group: $p < 0.001$ for free OXA and $p < 0.0001$ for both nanoparticle formulations (Fig. 7I). There was also a statistically significant difference when the treated groups were compared between each other: $p < 0.01$ for OXA x PLGA-PEG (OXA), $p < 0.0001$ for OXA x PLGA-PEG (OXA), and PLGA-PEG (OXA) x PLGA-PEG-FA (OXA). Regarding the analysis of the common pathway of apoptosis (caspase-3), the expression was increased in all groups when compared to the control: $p < 0.01$ for free OXA and $p < 0.0001$ for both nanoparticle formulations. The comparison between the treated groups showed a difference between the nanoparticle groups and free OXA group: $p < 0.0001$ for the two analyses (Fig. 7J).

The apoptosis-related gene expression analysis showed that only PLGA-PEG-FA (OXA) had expression of FADD when compared to the negative control ($p < 0.001$) (Fig. 7K). Also, for APAF-1, all treated groups had increased expression when compared to the negative control ($p < 0.0001$). In addition, the groups free OXA and PLGA-PEG-FA (OXA) also showed a significant difference between each other ($p < 0.001$) in terms of the expression of APAF-1 (Fig. 7K). The increase in mRNA expression for MDR1 and survivin was only observed for the OXA group in relation to control ($p < 0.01$ and $p < 0.001$, respectively). The same

results were obtained when OXA was compared with PLGA-PEG (OXA) and PLGA-PEG-FA (OXA) (Fig. 7).

CXCR4 expression was increased for free OXA and PLGA-PEG (OXA) in comparison to the control and for CCL22 expression only in the PLGA-PEG (OXA) group, $p < 0.0001$. Interestingly, PLGA-PEG-FA (OXA) did not increase the expression of these mRNAs.

4. Discussion

Using the double-emulsion solvent evaporation method of water-oil-water (W/O/W) allowed us to obtain nanoparticles with a range of sizes in which nanoparticles can be actively taken up by cells *via* endocytosis [34,35]. The nanoparticles showed a good stability since the zeta potential was between -20 mV and -24 mV, which are values that are typically indicative of high nanoparticles stability (Table 1) [36,37]. The differences in encapsulation efficiency were probably because of the chemistry of the formulated co-polymers. PLGA-PEG-FA nanoparticles loaded with the NIR dye and co-loaded with OXA did encapsulate almost 10% less of NIR dye than the PLGA-PEG nanoparticles. This is probably due to the encumbrance of the FA bound to the PLGA-PEG. The sizes obtained by TEM were slightly smaller (Fig. 2A-D) than those determined by DLS (Table 1). The difference is likely due to different sample preparation methods since hydrated particles were used for DLS, whereas rehydrated nanoparticles were used for TEM [38]. The pattern of release of OXA by the particulate systems, [PLGA-PEG (OXA) and PLGA-PEG-FA (OXA)], was continuous and slow, this shows that the drug was kept trapped inside the DDS for a long period of time [5,39]. PLGA-PEG-FA (OXA) released even slower than PLGA-PEG (OXA), this release pattern can ensure that the drug will not be released before its internalization in tumor cells, allowing to increase its accumulation in tumor tissues with the consequent decrease in possible side effects caused by OXA [5,40].

The binding and uptake tests complement each other and prove the

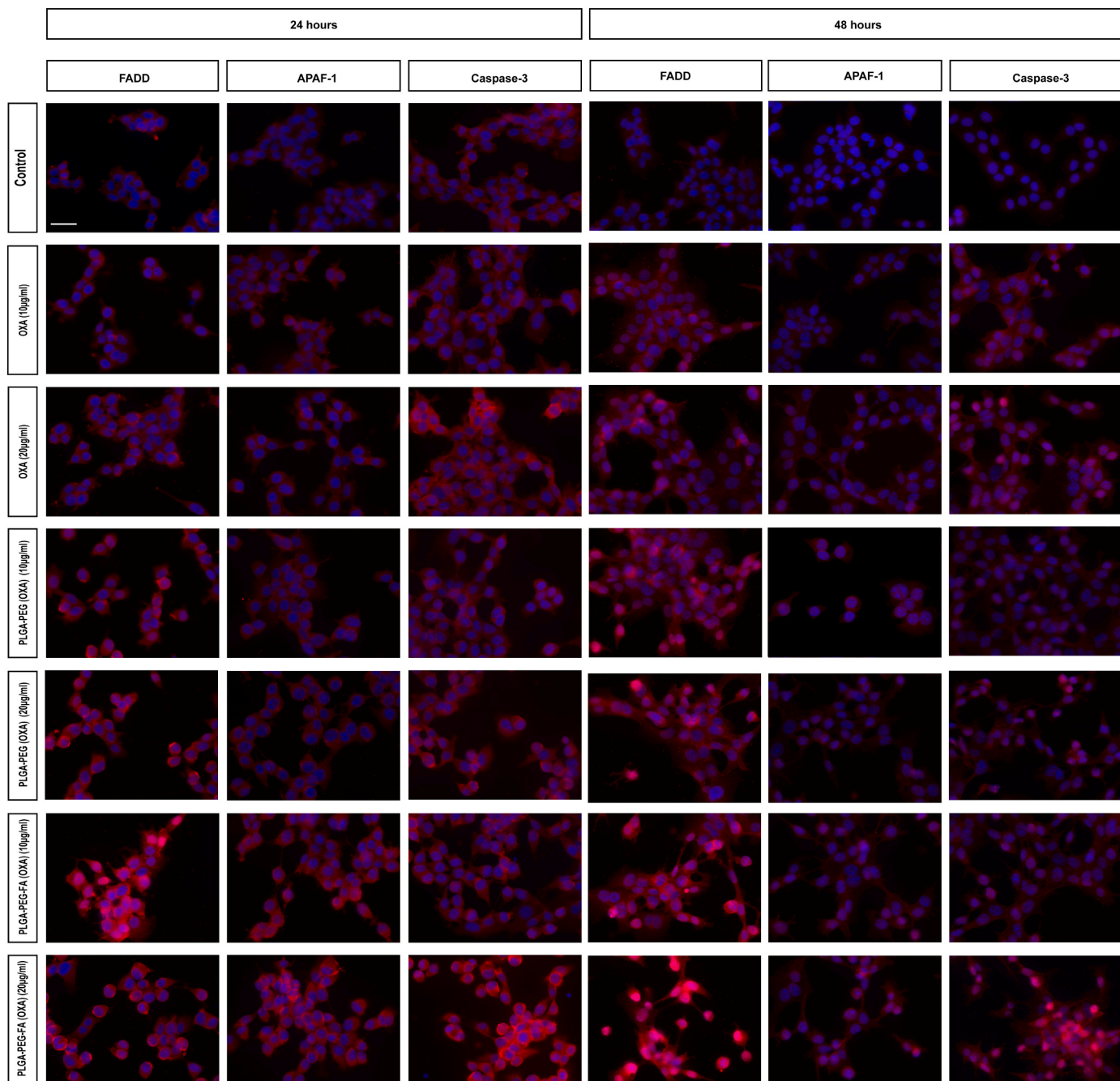


Fig. 5. Detection of FADD, APAF-1, and caspase-3 after 24 and 48 h of treatment. CT-26 cells stained with DAPI (blue) as well as anti-FADD, anti-APAF-1, or anti-caspase-3 antibodies (red). Scale bar: 50 μ m. (For interpretation of the references to colour in this figure legend, the reader is referred to the web version of this article.)

acid folic target's effectiveness in maximizing OXA activity. In this study, we were able to confirm that the system with FA works. During the same time period, PLGA-PEG-FA greatly improved the binding and internalization of the nanoparticles by tumor cells when compared to PLGA-PEG, which did not possess FA [41]. As CRC cells overexpress FA receptors, this system is of great use in the treatment of this kind of tumors [41]. The microscopic images corroborate these results and allow the visualization of the nanoparticles, due to the presence of the FA inside the cells [42,43].

Since nanoparticles, which contained FA for targeting purposes, were internalized at a higher rate, cytotoxicity and the percentage of cell death increased due to the improved effectiveness of the OXA treatment. The FA-containing DDS already induces cell death after 24 h. This

activity is sustained, showing higher rates after 48 h, the second time of analysis [44]. This initial activity of the tumor cells is not observed for free OXA, since the internalization of free OXA is not facilitated by the target, *i.e.* FA, and the tumor cells developed a resistance to treatment with OXA [42,45]. This evidence reveals the importance of using a DDS to circumvent treatment barriers, such as drug resistance.

Evasion of apoptosis, drug resistance, and metastasis are interconnected factors, which are present in tumor malignancy. These factors can be the reason for the failure of a cancer treatment, that, as a result, allow tumor progression or recurrence [7,46,47]. Therefore, DDSs with therapeutic action *via* induction of apoptosis are promising [48]. Our immunofluorescence data showed an increase in apoptosis in tumor cells when treated with PLGA-PEG-FA (OXA), when compared to free OXA.

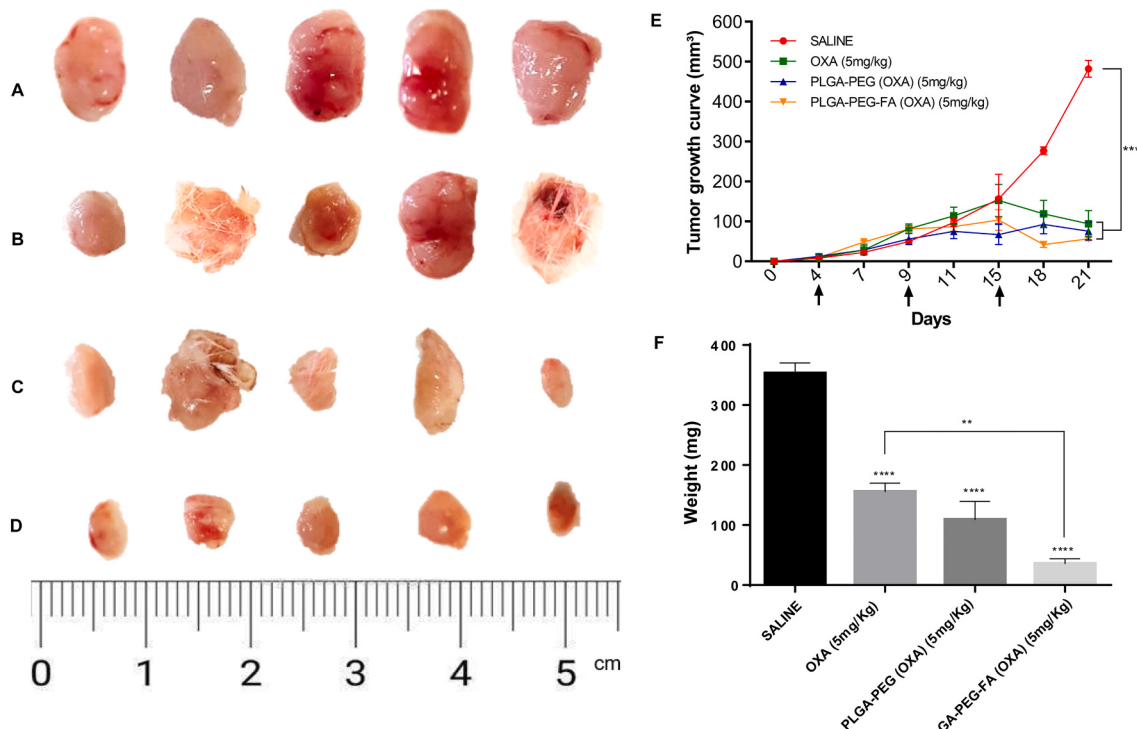


Fig. 6. Macroscopic results of the CRC *in vivo* xenograft model. Morphology of the tumors collected from Saline (A), OXA (5 mg/Kg) (B), PLGA-PEG (OXA) (5 mg/Kg) (C), and PLGA-PEG-FA (OXA) (5 mg/Kg) (D) groups. Tumor growth curve (E) and weight graph (F) of the xenograft tumors with different treatments. All treatment groups were compared with saline group. ** p < 0.01 and **** p < 0.0001.

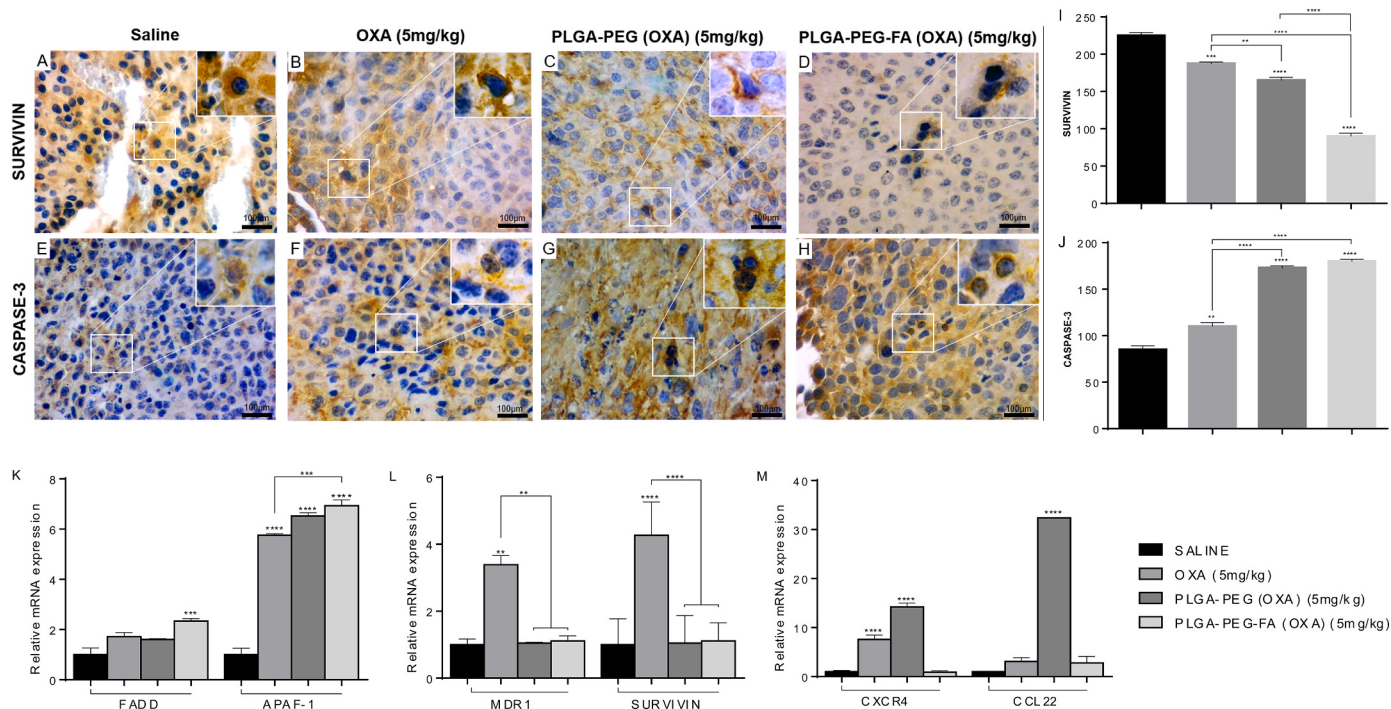


Fig. 7. Analysis of apoptosis, drug resistance, and metastasis factors. Representative images of immunohistochemistry of tumor fragments of mice treated with saline, OXA, and nanoparticles (A–H). Immunohistochemistry score by anti-survivin (I) and anti-caspase-3 (J). Relative mRNA expression by of FADD and APAF-1 (K), MDR1 and survivin (L), and CXCR4 and CCL22 (M) as determined by RT-PCR. All treatment groups were compared with the negative control group and between the treated groups. ** p < 0.01, *** p < 0.001, and **** p < 0.0001. Magnification (A–H): 40×.

Our *in vitro* results of apoptosis induction were confirmed *in vivo* by means of a regression of the tumor size. In relation to free OXA, tumor size was decreased by 3 times after treatment with PLGA-PEG-FA (OXA). Drug resistance is a known characteristic of treatment with OXA [49]. Our data shows decreased OXA resistance when cells are treated with PLGA-PEG-FA (OXA), which indicates that cells are more susceptible to the action of OXA when it is incorporated into the PLGA system targeted with FA. These results corroborate other studies and, thereby, confirm the efficiency of this target system and uptake by the cells *via* endocytosis [50,51].

The tumor microenvironment, invasion, and metastasis are also targets of antitumor therapies. Hence, we went beyond the study of apoptosis and drug resistance [52]. We also analyzed the expression of CXCR4, a chemokine receptor, overexpressed in metastases, tumor growth, proliferation, and invasion, and CCL22, a macrophage-derived chemokine that attracts regulatory T cells to the tumor microenvironment, thereby, decreasing anti-cancer immunity [53–56]. The groups treated with free OXA and PLGA-PEG (OXA) showed an increase for CXCR4 compared to the saline group, while treatment with PLGA-PEG-FA (OXA) did not show a difference. Regarding CCL22, only PLGA-PEG (OXA) increased levels in relation to the control. These results reveal that the PLGA-PEG-FA (OXA) DDS does not interfere in the expression of CXCR4 and CCL22 that are related to tumor microenvironment and tumor progression.

Our results showed that PLGA-PEG-FA increased the antitumor effectiveness of OXA by functioning as a facilitator of drug delivery in CRC. These results contribute to our understanding of the drug delivery mechanisms that underlie the antitumor effects of chemotherapy in nanoscale.

Supplementary data to this article can be found online at <https://doi.org/10.1016/j.msec.2020.111678>.

Funding sources

This work was supported by CAPES [grant numbers 88881.133518/2016-01 and 88881.119850/2016-01]; the European Union's Horizon 2020 research and innovation programme under the Marie Skłodowska Curie [grant numbers CANCER 777682, PAVE 861190, CAST 857894, PRISAR2 872860, SIMICA 852985 and ACORN 807281].

CRediT authorship contribution statement

Ana Luiza Oliveira: Conceptualization; Investigation; Formal analysis; Writing, original draft preparation; Writing, review and editing; Visualization.

Luana Zerillo: Investigation; Formal analysis; Writing, original draft preparation.

Luis Cruz: Supervision.

Timo Schomann: Investigation; Formal analysis; Writing, review and editing.

Alan Chan: Project administration; Funding acquisition.

Thaís Carvalho: Formal analysis.

Shirley Souza: Investigation;

Aurigena Araújo: Formal analysis.

Lioe-Fee de Geus-Oei: Supervision.

Raimundo Júnior: Conceptualization; Writing, review and editing; Supervision.

Declaration of competing interest

The authors declare that they have no known competing financial interests or personal relationships that could have appeared to influence the work reported in this paper.

References

- [1] E.J. Kuipers, W.M. Grady, D. Lieberman, T. Seufferlein, J.J. Sung, P.G. Boelens, C.J. H. van de Velde, T. Watanabe, *Nature Reviews Disease Primers* 1 (2015) 15065.
- [2] F. Bray, J. Ferlay, I. Soerjomataram, R.L. Siegel, L.A. Torre, A. Jamal, *CA Cancer J. Clin.* 68 (2018) 394–424.
- [3] A. Guerra, L.A.L. Soares, M.R.A. Ferreira, A.A. Araújo, H.A.O. Rocha, J.S. Medeiros, R.D.S. Cavalcante, R.F.A. Júnior, *Biomedicine & pharmacotherapy = Biomedecine & pharmacotherapie* 92 (2017) 696–706.
- [4] A.L.C. de S.L. Oliveira, R.F.d. Araújo Júnior, T. Gomes de Carvalho, A.B. Chan, T. Schomann, F. Tamburini, L.-F. de Geus-Oei, L.J. Cruz, *Pharmaceutics* 12 (2020) 193.
- [5] A.L.C.S.L. de Oliveira, A.M. dos Santos-Silva, A.A. da Silva-Júnior, V.B. Garcia, A. A. de Araújo, L.-F. de Geus-Oei, A.B. Chan, L.J. Cruz, R.F. de Araújo Júnior, *Journal of Nanoparticle Research* 22 (2020) 115.
- [6] R.S. Wong, *Journal of experimental & clinical cancer research: CR* 30 (2011) 87.
- [7] D. Hanahan, R.A. Weinberg, *Cell* 144 (2011) 646–674.
- [8] M.S. D'Arcy, *Cell Biol. Int.* 43 (2019) 582–592.
- [9] B.A. Carneiro, W.S. El-Deiry, *Nature reviews, Clin. Oncol.* 17 (2020) 395–417.
- [10] Y. Shi, B. Tang, P.-W. Yu, B. Tang, Y.-X. Hao, X. Lei, H.-X. Luo, D.-Z. Zeng, *PLoS One* 7 (2012), e51076.
- [11] T.V. Rakitina, I.A. Vasilevskaya, P.J. O'Dwyer, *Biochem. Pharmacol.* 73 (2007) 1715–1726.
- [12] B. Stordal, N. Pavlakis, R. Davey, *Cancer Treat. Rev.* 33 (2007) 347–357.
- [13] Z.P. Hong, L.G. Wang, H.J. Wang, W.F. Ye, X.Z. Wang, *Phytomedicine* 39 (2018) 168–175.
- [14] W. Cheng, J. Nie, N. Gao, G. Liu, W. Tao, X. Xiao, L. Jiang, Z. Liu, X. Zeng, L. Mei 27 (2017) 1704135.
- [15] N. Ashwanikumar, N.A. Kumar, S.A. Nair, G.S.V. Kumar, *Colloids Surf B: Biointerfaces* 122 (2014) 520–528.
- [16] W. Ni, Z. Li, Z. Liu, Y. Ji, L. Wu, S. Sun, X. Jian, X. Gao, *J. Pharm. Sci.* 108 (2019) 1284–1295.
- [17] C. Liang, H. Wang, M. Zhang, W. Cheng, Z. Li, J. Nie, G. Liu, D. Lian, Z. Xie, L. Huang, X. Zeng, *J. Colloid Interface Sci.* 525 (2018) 1–10.
- [18] Z. Eskandari, F. Kazdal, F. Bahadori, N. Ebrahimi, *Journal of Drug Delivery Science and Technology* 48 (2018) 393–402.
- [19] X. Luo, Y. Yang, F. Kong, L. Zhang, K. Wei, *Int. J. Pharm.* 564 (2019) 340–349.
- [20] X. Song, J. Wang, Y. Xu, H. Shao, J. Gu, *Colloids Surf. B: Biointerfaces* 180 (2019) 110–117.
- [21] A. Banerjee, S. Pathak, V.D. Subramanium, D.G. Murugesan .R., R.S. Verma, *Drug Discov Today* 22 (2017) 1224–1232.
- [22] W. Cheng, X. Zeng, H. Chen, Z. Li, W. Zeng, L. Mei, Y. Zhao, *ACS Nano* 13 (2019) 8537–8565.
- [23] Y. Wang, P. Li, L. Chen, W. Gao, F. Zeng, L.X. Kong, *Drug Delivery* 22 (2015) 191–198.
- [24] M.M. El-Hammadi, Á.V. Delgado, C. Melguizo, J.C. Prados, J.L. Arias, *Int. J. Pharm.* 516 (2017) 61–70.
- [25] L.J. Cruz, P.J. Tacken, F. Rueda, J.C. Domingo, F. Albericio, C.G. Figdor, *Methods Enzymol.* 509 (2012) 143–163.
- [26] M.V.d.M. Ribeiro, I.d.S. Melo, F.d.C.d.C. Lopes, G.C. Moita, *Brazilian Journal of Pharmaceutical Sciences* 52 (2016) 741–750.
- [27] S.H. Boddu, R. Vaishya, J. Jwala, A. Vadlapudi, D. Pal, A.K. Mitra, 2 (2012) 068–075.
- [28] P. García-Manrique, N.D. Machado, M.A. Fernández, M.C. Blanco-López, M. Matos, G. Gutiérrez, *Colloids Surf. B: Biointerfaces* 186 (2020) 110711.
- [29] W. Zhang, F. Wang, X. Hu, J. Liang, B. Liu, Q. Guan, S. Liu, *Oncol. Lett.* 17 (2019) 815–822.
- [30] L. Liu, P.A. Mayes, S. Eastman, H. Shi, S. Yadavalli, T. Zhang, J. Yang, L. Seestaller-Wehr, S.Y. Zhang, C. Hopson, L. Tsvetkov, J. Jing, S. Zhang, J. Smothers, A. Hoos, *Clin. Cancer Res.* 21 (2015) 1639–1651.
- [31] Y. Liu, N. Zhang, Q. Cao, X. Cui, Q. Zhou, C. Yang, *Biomedicine & pharmacotherapy = Biomedecine & pharmacotherapie* 90 (2017) 47–52.
- [32] H. Liu, H.W. Xu, Y.Z. Zhang, Y. Huang, G.Q. Han, T.J. Liang, L.L. Wei, C.Y. Qin, C. K. Qin, *World J. Gastroenterol.* 21 (2015) 10367–10374.
- [33] E. Charafe-Jauffret, C. Tarpin, V.-J. Bardou, F. Bertucci, C. Ginestier, A.-C. Braud, B. Puig, J. Geneix, J. Hassoun, D. Birnbaum, J. Jacquemier, P. Viens, *J. Pathol.* 202 (2004) 265–273.
- [34] L. Shang, K. Nienhaus, G.U. Nienhaus, *J. Nanobiotechnology* 12 (2014) 5.
- [35] J.P. Marshalek, P.S. Sheeran, P. Ingram, P.A. Dayton, R.S. Witte, T.O. Matsunaga, *J. Control. Release* 243 (2016) 69–77.
- [36] V. Ayala, A.P. Herrera, M. Latorre-Esteves, M. Torres-Lugo, C. Rinaldi, *J. Nanopart. Res.* 15 (2013) 1874.
- [37] S. Bhattacharjee, *J. Control. Release* 235 (2016) 337–351.
- [38] R.F. Domingos, M.A. Baalousha, Y. Ju-Nam, M.M. Reid, N. Tufenkji, J.R. Lead, G. Leppard, K.J. Wilkinson, *Environmental Science & Technology* 43 (2009) 7277–7284.
- [39] S.A. Sufi, M. Hoda, S. Pajaniradje, V. Mukherjee, S.M. Coumar, R. Rajagopalan, *Int. J. Pharm.* 588 (2020) 119738.
- [40] B. Gibbens-Bandala, E. Morales-Avila, G. Ferro-Flores, C. Santos-Cuevas, L. Meléndez-Alafort, M. Trujillo-Nolasco, B. Ocampo-García, *Mater. Sci. Eng. C* 105 (2019) 110043.
- [41] A. Narmani, M. Kamali, B. Amini, A. Salimi, Y. Panahi, *Process Biochem.* 69 (2018) 178–187.
- [42] A. Akbarian, M. Ebtekar, N. Pakravan, Z.M. Hassan, *Int. J. Biol. Macromol.* 152 (2020) 90–101.

- [43] J. Hu, J.D. Obayemi, K. Malatesta, A. Košmrlj, W.O. Soboyejo, Mater. Sci. Eng. C 88 (2018) 32–45.
- [44] Z. Wang, X. Duan, Y. Lv, Y. Zhao, Life Sci. 239 (2019) 117013.
- [45] W. Gao, X. Jia, J. Wu, Y. Song, J. Yin, M. Zhang, N. Qiu, X. Li, P. Wu, X. Qi, Z. Liu, Journal of Drug Delivery Science and Technology 54 (2019) 101349.
- [46] B.D. Kurmi, P. Patel, R. Paliwal, S.R. Paliwal, Journal of Drug Delivery Science and Technology 57 (2020) 101682.
- [47] C. Box, S.J. Rogers, M. Mendiola, S.A. Eccles, Semin. Cancer Biol. 20 (2010) 128–138.
- [48] M.C. Pfeffer, T.K.A. Singh, International Journal of Molecular Sciences, 19, 2018.
- [49] D.B. Longley, P.G. Johnston, J. Pathol. 205 (2005) 275–292.
- [50] H. Tonbul, A. Sahin, E. Tavukcuoglu, G. Esenagli, Y. Capan, Journal of Drug Delivery Science and Technology 54 (2019) 101380.
- [51] J.L. Markman, A. Rekechenetskiy, E. Holler, J.Y. Ljubimova, Adv. Drug Deliv. Rev. 65 (2013) 1866–1879.
- [52] F. Guo, Y. Wang, J. Liu, S.C. Mok, F. Xue, W. Zhang, Oncogene 35 (2016) 816–826.
- [53] E. Martinenaite, S. Munir Ahmad, M. Hansen, Ö. Met, M.W. Westgaard, S. K. Larsen, T.W. Klausen, M. Donia, I.M. Svane, M.H. Andersen, Oncoimmunology 5 (2016) e1238541.
- [54] A. Maolake, K. Izumi, K. Shigehara, A. Natsagdorj, H. Iwamoto, S. Kadomoto, Y. Takezawa, K. Machioka, K. Narimoto, M. Namiki, W.-J. Lin, G. Wufuer, A. Mizokami, Oncotarget 8 (2017) 9739–9751.
- [55] C. Xu, L. Zheng, D. Li, G. Chen, J. Gu, J. Chen, Q. Yao, Life Sci. 208 (2018) 333–340.
- [56] M.V. Céspedes, U. Unzueta, P. Álamo, A. Gallardo, R. Sala, I. Casanova, M. A. Pavón, M.A. Mangues, M. Trías, A. López-Pousa, A. Villaverde, E. Vázquez, R. Mangues, Nanomedicine: Nanotechnology, Biology and Medicine 12 (2016) 1987–1996.